Electronic Research Archive

https://www.aimspress.com/journal/era

ERA, 34(2): 1209–1237.
DOI: 10.3934/era.2026056
Received: 08 January 2026
Revised: 28 January 2026
Accepted: 03 February 2026
Published: 06 February 2026

Research article

Solving an inverse source problem for nonlocal diffusion-wave equations through Laplace-based physics-informed neural networks

Weiyue Sun[1], **Changxin Qiu**[2,*] **and Zhiyuan Li**[2,*]

[1] School of Accounting, Ningbo University of Finance and Economics, Ningbo 315175, China
[2] School of Mathematics and Statistics, Ningbo University, Ningbo 315211, China

* **Correspondence:** Email: qiuchangxin@nbu.edu.cn, lizhiyuan@nbu.edu.cn.

Abstract: This work investigates the nonlocal diffusion-wave equation governed by the time-fractional Caputo derivative. We first establish that the solution is t-analytic through the application of Fourier expansion and the properties of the Mittag-Leffler functions. Building on this, we apply the Laplace transform to demonstrate the subordination principle for solutions of parabolic and hyperbolic equations in the context of the nonlocal diffusion-wave equation. Second, we prove the uniqueness and conditional stability of a solution to an inverse problem involving the determination of the spatially varying source term based on interior information from a subdomain. We alslo introduce a novel framework termed Laplace-based physics-informed neural networks (L-PINNs), which is tailored for determining source terms in nonlocal diffusion-wave systems. We substantiate the proposed approach through a series of numerical experiments, demonstrating its superior accuracy and computational efficiency.

Keywords: nonlocal diffusion-wave equation; inverse source problem; subordination principle; Laplace transform; Laplace-based physics-informed neural networks

1. Introduction

This work investigates the initial-boundary value problem associated with the nonlocal diffusion-wave equation. Let $\Omega \subset \mathbb{R}^d$ $(d \geq 1)$ be a bounded domain possessing a sufficiently smooth boundary $\partial\Omega$. The governing system is given by

$$\begin{cases} (\partial_t^\alpha - \Delta)u(x,t) = R(x,t)f(x) & \text{in } \Omega \times [0,+\infty), \\ u(x,0) = u_0(x),\ u_t(x,0) = u_1(x) & \text{in } \Omega, \\ u(x,t) = 0 & \text{on } \partial\Omega \times [0,+\infty), \end{cases} \tag{1.1}$$

where the operator ∂_t^α denotes the Caputo fractional derivative of order $\alpha \in (1, 2)$. This derivative is explicitly defined as

$$\partial_t^\alpha u(x,t) = \frac{1}{\Gamma(2-\alpha)} \int_0^t (t-\tau)^{1-\alpha} \partial_\tau^2 u(x,\tau) \mathrm{d}\tau, \quad 1 < \alpha < 2. \tag{1.2}$$

By generalizing classical integer-order models, fractional differential equations have become essential tools for modeling complex phenomena in diverse disciplines, ranging from fluid dynamics and continuum mechanics to biological systems and chemical kinetics [1–4]. In recent years, their profound physical background and rich theoretical connotations have garnered increasing attention.

For mathematical research purposes, the nonlocal diffusion-wave equation has long piqued the interest of a diverse group of mathematicians. For numerical methods and mathematical analyses on solving fractional differential equations, we refer to the references [5–10]. In [5], the Laplace transform method was combined with two- or three-level finite difference schemes in time to solve fractional differential equations. In [6], two finite difference schemes were developed to solve a specific class of initial-boundary-value, time-fractional diffusion-wave equations. Furthermore, [8, 10] employed the local discontinuous Galerkin finite element method and the novel L1-predictor-corrector method, respectively, to solve Caputo-type partial differential equations.

Meanwhile, the inverse source problems of nonlocal partial differential equations have been heavily studied in recent years. In this paper, we specifically focus on the inverse problem of determining the coefficient $f(x)$ and solution $u(x,t)$ from additional measurements of $u(x,t)$ in $\omega \times (0,\infty)$, where ω is a subdomain of Ω, assuming that the initial value $u_0(x)$, coefficient $R(x,t)$, and fractional order α are already known. More precisely, we focus on the inverse source problem of the system (1.1) in the following formualtion:

Problem 1. *Let $u_0 = u_1 = 0$ in Ω and $R \in C(0,\infty; H^2(\Omega))$ be known with $R(x,0) \neq 0$. Let ω be a subdomain of Ω. We propose the following*

i. (Uniqueness) Given the interior observation $u(x,t)$, $(x,t) \in \omega \times (0,\infty)$, we investigate whether the measurement uniquely determines the source function $f(x)$, $x \in \Omega$.

ii. (Stability) We establish a conditional stability for the forward mapping $u_{\omega\times(0,\infty)} \mapsto f$.

iii. (Reconstruction) The primary objective of this work is to construct a computationally efficient numerical solver for the reconstruction of the unknown source term f.

The inverse problem with separable source terms is a standard and well-studied formulation in the mathematical theory of inverse problems for evolution equations. It naturally arises in scenarios such as photoacoustic or thermoacoustic tomography, where the temporal excitation pattern source can be characterized independently, whereas its spatial distribution must be inferred from additional measurements; see [11–13] for the mathematical well-posedness and analysis.

To the best of the authors' knowledge, prior studies on inverse problems pertaining to nonlocal differential equations have primarily concentrated on the case where $0 < \alpha < 1$. Various theoretical and numerical strategies have been proposed to address this challenge. For instance, Carleman estimates were utilized by Zhang et al. [14] to analyze the half-order fractional diffusion case. In the context of stochastic equations, Niu et al. [15] developed a regularized reconstruction scheme for random source problems. From an optimization perspective, Jiang et al. [16] recast the problem to apply an

iterative thresholding algorithm. Moreover, approaches based on a posteriori boundary measurements were investigated by Janno et al. [17] to recover space- or time-dependent sources. Furthermore, methods such as a reproducing kernel Hilbert Space (RKHS), the separation of variables, and Tikhonov regularization have been successfully applied to time-fractional source identification in [18, 19].

Despite the contributions of researchers such as Cheng et al. [20], Hu et al. [21], Liao et al. [22], Yan et al. [23], and Yamamoto [24], theoretical advancements in the determination of spatially varying sources for $\alpha \in (1, 2)$ remain limited. More precisely, research on identifying spatially dependent sources in fractional diffusion equations has yielded several unique determination theorems and numerical approaches. Cheng et al. [20] established that when the coefficients are t-independent, the uniqueness of source identification can be guaranteed by leveraging the analyticity of the solution and a newly formulated unique continuation principle. For numerical reconstruction, Liao et al. [22] developed a Levenberg–Marquardt algorithm capable of simultaneously inverting for both the fractional order and the spatial source term. Furthermore, Yan et al. [23] addressed the more challenging scenario of incomplete and noisy data, focusing on recovering a space-dependent source in a symmetric time-fractional diffusion-wave equation from partial boundary measurements. The uniqueness proof in this work relied on the Titchmarsh convolution theorem and the Duhamel principle. Liu et al. [21] investigated the identification of the moving source profiles in fractional diffusion-wave equations. They validated the unique identification of different source profiles using the unique continuation principle. In [25], the authors investigated the stochastic time-fractional diffusion-wave equation in Hilbert space and applied it to the inverse source problem. In [24], the authors have demonstrated the uniqueness of the inverse source problem in determining the spatially varying factor through the decay of data as time approaches infinity, assuming that the source is inactive during the observation period. The scope of inverse analysis extends beyond source terms to encompass the recovery of fractional exponents, initial conditions, and variable coefficients. A holistic perspective on these topics is provided in the reviews by [26].

To the authors' knowledge, most research on the inverse source problem for fractional diffusion-wave equations assumes a source term that is separable in space and time. Currently, there is no research specifically addressing the form $F = R(x, t)f(x)$ in the initial-boundary value system (1.1). Moreover, the existing literature on fractional inverse source problems has predominantly focused on theoretical uniqueness analysis, primarily due to the lack of tools such as the Carleman estimate. By assuming a temporally and spatially separable source term, we investigate the conditional stability of determining the source term based on interior observations. This represents an innovative aspect of our article.

In parallel, given the intricacies involved in discretizing fractional partial differential equations, data-driven approaches and deep learning techniques have gained significant traction as powerful alternatives to traditional methods. Guo et al. [27] proposed a sampling-based machine learning method that computes the fractional derivative of deep neural network (DNN) output via a Monte Carlo. Pang et al. [28] proposed fractional physics-informed neural networks (fPINNs), which approximate fractional derivatives by numerically discretizing the fractional operator and utilizing automatic differentiation to obtain integer-order derivatives of the network. Hou et al. [29] employed Hermite interpolation techniques to construct an approximation scheme for fractional derivatives and integrated this scheme with deep neural networks to achieve a high-precision solver. Similarly, Ma et al. [30] presented a scheme that combines neural networks with interpolation approximations of

fractional derivatives. Chen et al. [31] proposed a physics-informed neural networks based on Laplace transform to solve the nonlinear coefficient inverse problem for acoustic equation. Qu et al. [32] modeled shallow neural networks using sine and cosine functions as neurons, and the authors of [33] built neural network based on a Legendre polynomials. To reduce the number of approximate points for discrete fractional operators and to enhance training efficiency, Wang et al. [34] introduced a model solver that integrates fPINNs with the spectral collocation method. Additionally, the works in [35, 36] demonstrated the effectiveness of a dual-network structure based on neural network parallelism and the fractional Chebyshev deep neural network (FCDNN) in addressing fractional differential equations. Despite the numerous machine learning methods currently applied to fractional differential equations, there remains a need to explore more flexible and efficient neural network approaches for the inverse source problem with $F = R(x,t)f(x)$ for fractional diffusion-wave equations.

In this paper, we also propose Laplace-based physics-informed neural networks (L-PINNs) for solving the inverse problem of time-fractional differential equations. Our approach transforms the original fractional differential equations into elliptic equations within the Laplace domain using Laplace transforms. This transformation facilitates the use of physics-informed neural networks (PINNs) and overcomes the constraints posed by automatic differentiation in addressing fractional problems. Unlike methods that combine neural networks with numerical approximations of fractional derivatives, L-PINNs eliminate the numerical approximation step through the use of the Laplace transform. This significantly reduces computational costs during network training and simplifies the process of solving high-dimensional problems. In comparison to the f-PINNs method, our network has been shown to effectively address the inverse problem for a class of source terms on both one- and two-dimensional (1D and 2D) problems when additional measurements are employed.

The primary technical challenges addressed in this work are as follows:

i. The presence of a time-dependent function $R(x,t)$ in the source term makes the usual analytical technique used in [20, 37] primarily because we cannot leverage the Duhamel principle to transform the inverse source problem into an initial value inversion problem.

ii. Due to the lack of suitable Carleman estimates, we are unable to derive stability estimates for the inverse source problem in the same manner as for classical partial differential equations.

The principal contributions of this work can be summarized as follows:

i. We prove the uniqueness of the inverse source term by applying the subordination principle, which links the solution of the fractional diffusion-wave equation to that of the hyperbolic equation.

ii. We derive a stability estimate for the solution of problem (1.1) with respect to the interior measurements, utilizing the subordination relationship between fractional and classical parabolic equations.

iii. Our approach converts fractional equations to elliptic ones via Laplace transforms, enabling PINNs application without fractional derivative approximations, simplifying high-dimensional problem solving and reducing costs.

This paper is structured to first provide the necessary preliminaries and state our main results in Section 2. Building on this foundation, Section 3 completes the theoretical analysis by establishing the subordination principle for the solution of system (1.1). The focus then shifts to the numerical

methodology in Section 4, where we detail the L-PINNs framework and its specific application to the time-fractional inverse source problem. In Section 5, the proposed algorithm is validated through comprehensive numerical experiments using both one- and two-dimensional benchmarks. Finally, concluding remarks are drawn in Section 6.

2. Preliminaries and main results

2.1. Settings

A key step in our investigation involves applying the Laplace transform. This allows us to prove that the source term is uniquely determined by data observed within the interior domain. Here we define the Laplace transform of a function,

$$\mathcal{L}\{\varphi; s\} = \int_0^\infty \varphi(t)e^{-st}dt, \quad s > s_0,$$

and sometimes for convenience, we also denote the Laplace transform as $\widehat{\varphi}(s)$ or $\mathcal{L}\varphi$. To this end, the additional assumption on the source function $R(x, t)$ is required.

Assumption 1.

i. $R(x,t) \in C((0,\infty); H^2(\Omega))$. *The source term* $R(x,t) : (0,\infty) \to H^2(\Omega)$ *can be analytically extended to the right-half complex plane* $\Re z > 0$, *and we still denote the extended function as* $R(x,t)$ *if no conflict occurs.*

ii. We assume the extended source function R is of exponential growth with respect to variable $z \in \mathcal{S}$, *that is,* $|R(x,z)| \le Ce^{C|z|}$, $\Re z > 0$, *where the constant* $C > 0$ *is independent of* z *and* $x \in \overline{\Omega}$.

iii. The Laplace transform $\widehat{R}(x,s)$ *can be analytically extended to the complex sector*

$$\mathcal{S} = \{z \in \mathbb{C} \setminus \{0\}; |argz| < \theta_0\}, \tag{2.1}$$

where the argument $\theta_0 \in (\frac{\pi}{2}, \pi)$ *holds, and it is such that*

$$\lim_{t\to 0} \int_{s_0-i\infty}^{s_0+i\infty} \widehat{R}(x, s^{\frac{2}{\alpha}})e^{st}ds \neq 0. \tag{2.2}$$

Next, we will present several essential settings and lemmas associated with the fractional operators defined in Section 1. These foundational elements will be instrumental in the subsequent analysis. We begin by recalling relevant properties of the Mittag-Leffler functions.

$$E_{\alpha,\gamma}(z) := \sum_{j=0}^{\infty} \frac{z^j}{\Gamma(\alpha j + \gamma)}, \quad z \in \mathbb{C},$$

where $\alpha > 0$, and $\gamma \in \mathbb{R}$. It is known that $E_{\alpha,\gamma}(z)$ is an analytic function in the complex plane $\mathbb{C}$. We first draw upon the asymptotic estimates from Podlubny [38].

Lemma 1. *Suppose that $\alpha \in (0,2)$, and $\gamma \in \mathbb{R}$. If the parameter μ satisfies the condition $\frac{\pi\alpha}{2} < \mu < \min\{\pi, \pi\alpha\}$, then there exists a constant C depending on α, γ, and μ such that the following estimate holds:*

$$|E_{\alpha,\gamma}(z)| \le C(1+|z|)^{-1} \quad \text{for all } z \text{ with } \mu \le |\arg z| \le \pi.$$

It is easily seen that the Laplace transform of the Mittag-Leffler function $E_{\alpha,1}(-t^\alpha)$ is such that:

$$\mathcal{L}\{E_{\alpha,1}(-t^\alpha); s\} = \frac{s^{\alpha-1}}{s^\alpha + 1}$$

and

$$\mathcal{L}\{t^{\alpha-1}E_{\alpha,\alpha}(-t^\alpha); s\} = \frac{1}{s^\alpha + 1}.$$

We now recall the property of the Laplace transform acting on the fractional derivative,

$$\widehat{\partial_t^\alpha \phi}(s) := \mathcal{L}(\partial_t^\alpha \phi) = s^\alpha \widehat{\phi}(s). \tag{2.3}$$

On the basis of the above notations and settings, we can show that the assumption (2.2) on the source function R can be satisfied. We give the following example.

Example 2.1. *By letting $R(x,t) = t^{\alpha/2-1}E_{\alpha/2,\alpha/2}(-t^{\alpha/2})$, we see that the Laplace transform of the source term R with respect to t can be calculated as follows:*

$$\widehat{R}(x,s) = \frac{1}{s^{\alpha/2}+1},$$

which implies $\widehat{R}(x, s^{\frac{2}{\alpha}}) = 1/(s+1)$. Then, we see that

$$e^{-t} = \frac{1}{2\pi i}\int_{s_0-i\infty}^{s_0+i\infty} \frac{1}{s+1}e^{st}ds.$$

Of course, $e^0 = 1 \neq 0$. We see that the assumption (2.2) *can be satisfied.*

2.2. Main results

We can have the first answer of the above inverse source Problem 1, that is, the uniqueness on determining the unknown source, by constructing a subordination principle to the solution of hyperbolic equations for nonlocal diffusion-wave equations.

Theorem 1. *We suppose $F(x,t)$ is of the form $R(x,t)f(x)$ in the problem* (1.1)*, and we suppose $R(x,t)$ is known as a function in the space $C([0,T]; H^2(\Omega))$ such that $R(x,0) \neq 0$. We let the function $u \in H_\alpha\left(0,T; L^2(\Omega)\right) \cap L^2\left(0,T; H_0^1(\Omega) \cap H^2(\Omega)\right)$ be the solution to the problem* (1.1) *with $f \in H_0^1(\Omega)$, and $u_0 = u_1 = 0$. Then, $u(x,t) = 0$, $(x,t) \in \omega \times (0,T)$ implies $f = 0$ in Ω.*

Furthermore, when the source function R is spatially independent, we can leverage the subordination principle connecting the fractional system (1.1) to its parabolic counterpart. Using this approach, log-type stability for the inverse source problem 1 is established under an appropriate norm.

Theorem 2. *Adopting the hypotheses outlined in Theorem 1, let the pair (u, f) denote a solution to the inverse source problem 1 consistent with the observed data. We then have*

$$\|f\|_{L^2(\Omega)} \leq C|\log \|\mathcal{L}^{-1}\{\widehat{u}(\cdot, s^{\frac{1}{\alpha}}); t\}\|_{H^1(0,T;H^2(\omega))}|^{-\beta}, \tag{2.4}$$

where $\beta > 0$, and the positive constant C is independent of u and f.

The aforementioned estimation formula stems from a thorough analysis of the characteristics and attributes of the observed data within the frequency domain. However, when attempting to translate (2.4) into estimates in the time domain, we encountered significant technical obstacles. Specifically, the complexity of the inversion Laplace transform hinders our ability to simplify the estimation formula derived in the frequency domain into a more intuitive and comprehensible form within the time domain. In light of this challenge, we have incorporated it into our future research plans.

3. Analysis of the main results

The rigorous proofs for the two principal findings are provided below. For this, we will first show the t-analyticity of the solution u to the initial-boundary value problem (1.1) under the assumptions in Theorems 1 and 2.

3.1. Analyticity of solutions

We first recall some standard function spaces. Let $L^2(\Omega)$ denote the usual space of square-integrable functions endowed with the inner product $\langle \cdot, \cdot \rangle_{L^2(\Omega)}$, abbreviated as $\langle \cdot, \cdot \rangle$. The conventional Sobolev spaces are denoted by $H^\ell(\Omega)$ and $H_0^k(\Omega)$. On the domain $\mathcal{D}(A_0) = H_0^1(\Omega) \cap H^2(\Omega)$, we define the operator A_0 by

$$A_0 u(x) := -\Delta u(x). \tag{3.1}$$

The operator A_0 defined in this manner is symmetric and uniformly elliptic. By $\{\lambda_n, \varphi_n\}_{n=1}^\infty$, we denote the Dirichlet eigensystem of A_0, where $0 < \lambda_1 \leq \lambda_2 \leq \cdots$, and the corresponding eigenfunctions $\{\varphi_n\}_{n=1}^\infty$ form an orthonormal basis of $L^2(\Omega)$. Next, we follow the treatment in [20] to define the fractional power A_0^γ of the operator A_0,

$$A_0^\gamma u := \sum_{n=1}^\infty \langle u, \varphi_n \rangle \lambda_n^\gamma \varphi_n, \quad u \in D\left(A_0^\gamma\right),$$

where $D\left(A_0^\gamma\right)$ becomes a Hilbert space,

$$D\left(A_0^\gamma\right) := \left\{ \psi \in L^2(\Omega); \sum_{n=1}^\infty \lambda_n^{2\gamma} |\langle u, \varphi_n \rangle_{L^2(\Omega)}|^2 < \infty \right\},$$

if it is equipped with the norm

$$\|\psi\|_{D(A_0^\gamma)} := \left[\sum_{n=1}^\infty |\langle \psi, \varphi_n \rangle \, \lambda_n^\gamma|^2 \right]^{\frac{1}{2}}.$$

It is easily seen that $D\left(A_0^\gamma\right) \subseteq H^{2\gamma}(\Omega)$ for $\gamma > 0$; see [37]. More specially, one can check that

$$D(A_0) = H^2(\Omega) \cap H_0^1(\Omega) \text{ and } D\left(A_0^{\frac{1}{2}}\right) = H_0^1(\Omega). \tag{3.2}$$

For any z belonging to the sector $\mathcal{S}$ described in (2.1), we introduce the operator $S(z) : L^2(\Omega) \to L^2(\Omega)$ defined by

$$S(z)\varphi := \sum_{n=1}^{\infty} E_{\alpha,1}(-\lambda_n z^\alpha)\langle \varphi, \varphi_n\rangle \varphi_n, \quad a \in L^2(\Omega). \tag{3.3}$$

Moreover, the asymptotic estimate provided in Lemma 1 justifies differentiating the operator $S(z)$ term by term. This operation yields the following expression:

$$S'(z)\varphi = -\sum_{n=1}^{\infty} \langle \varphi, \varphi_n\rangle z^{\alpha-1}\lambda_n E_{\alpha,\alpha}(-\lambda_n z^\alpha)\varphi_n, \quad \varphi \in L^2(\Omega).$$

Based on this representation, the requisite asymptotic bounds for operators $S(z)$ and $S'(z)$ are derived from the work of Cheng and Li [20].

Lemma 2. *With $\gamma \in [0, 1]$ and z belonging to the sector S as described in* (2.1)*, $S(z)$ and its derivative $S'(z)$ satisfy the estimates below:*

$$\begin{aligned} \left\|A_0^{\gamma-1} S(z)\right\|_{L^2(\Omega)\to L^2(\Omega)} &\le C|z|^{-\alpha(\gamma-1)}, \\ \left\|A_0^{\gamma-1} S'(z)\right\|_{L^2(\Omega)\to L^2(\Omega)} &\le C|z|^{\alpha(1-\gamma)-1}, \end{aligned} \tag{3.4}$$

where the constant C is positive and only depends on d, α, Ω, and γ.

Based on the above estimates for the solution operators, we can now establish the well-posedness of the solution u to the problem (1.1).

Lemma 3. *Under Assumption 1, the initial-boundary value problem* (1.1) *admits a unique solution $u \in L^2(0, T; D(A_0)) \cap C\left([0, T]; L^2(\Omega)\right) \cap H_\alpha\left(0, T; L^2(\Omega)\right)$, and*

$$\|u\|_{L^2(0,T;D(A_0))} + \|u\|_{H_\alpha(0,T;L^2(\Omega))} \le C_T \|f\|_{H^2(\Omega)}. \tag{3.5}$$

Furthermore, the mapping $t \in (0, T] \mapsto u(t) \in D(A_0)$ admits an analytic extension to the sector S given by (2.1)*. The properties of this extended function $u : (0, \infty) \to D(A_0)$ imply that*

$$\|u(t)\|_{D(A_0)} \le C\|f\|_{H^2(\Omega)} \min\{1, t^{-\alpha}\} e^{Ct}, \quad t > 0.$$

Throughout this paper, we use $C > 0$ and $C_T > 0$ to represent generic constants. The constant C is independent of t, T, and u, though it may depend on α, d, and Ω. The constant C_T, on the other hand, is independent of t and u but may additionally depend on the final time T.

Proof. We have the representation formula of the solution to the problem

$$u(t) = -\int_0^t A_0^{-1} S'(t-\tau) F(\tau) d\tau, \quad 0 < t < T. \tag{3.6}$$

After taking the change of variables, we see that

$$u(t) = t\int_0^1 A_0^{-1} S_1'(tr) F(t(1-r)) dr. \tag{3.7}$$

Next, we extend the real variable t in (3.7) from the interval $(0, T)$ to the sector S. We define $u_\varepsilon(z)$ as follows:

$$\tilde{u}_\varepsilon(z) = -z \int_\varepsilon^1 A_0^{-1} S'(zr) F(z(1-r)) dr. \tag{3.8}$$

In view of the definition in (3.3) and the properties of the Mittag-Leffler functions in Lemma 1, we see that $u_\varepsilon(z)$ defined above in (3.8) is analytic with respect to the variable $z \in K \subset\subset \mathcal{S}$. Moreover, it is not difficult to check that u_ε uniformly converges to $u(x, z)$:

$$\tilde{u}(z) = -z \int_0^1 A_0^{-1} S_1'(zr) F(z(1-r)) dr$$

for any subset compacted in the sector S. The details of the proof of this statement are as follows.

For the analyticity of u_ε, we have

$$\begin{aligned} \|\tilde{u}_\varepsilon(z)\|^2_{D(A_0^\gamma)} \leq & |z^2| \int_\varepsilon^1 \|A_0^{\gamma-1} S'(rz)\| \|F((1-r)z)\| dr \\ \leq & C|z|^{2+\alpha(1-\gamma)} \int_\varepsilon^1 r^{\alpha(1-\gamma)-1} dr e^{|z|} \|f\| < \infty. \end{aligned}$$

We see from Weierstrass theorem that $\tilde{u}_\varepsilon$ is analytic in $z \in K$. Because K can be arbitrarily chosen, we have that $\tilde{u}_\varepsilon$ is analytic in the sector $\mathcal{S}$. Moreover, by restricting the complex-valued variable $z \in \mathcal{S}$ to the real interval $(0, T)$, we can conclude that $u(t)$ is the unique solution to the integral equation (3.6).

Additionally, the presented argument implies the analytic extensibility of $u(t)$ to a function $u(t) : (0, \infty) \to D(A_0)$, and the extended solution fulfills the following growth estimate:

$$\|A_0 u(t)\|_{L^2(\Omega)} \leq C\|f\| e^{MT}, \quad 0 < t < T.$$

This completes the proof of the lemma.

3.2. Proof of the uniqueness result

Given the t-analyticity of the solution to (1.1), the mapping $u : (0, T) \to H^2(\Omega) \cap H_0^1(\Omega)$ admits an analytic continuation to $t \in (0, \infty)$. Consequently, we may apply the Laplace transform to both sides of (1.1). To proceed, we note the Laplace transform formula for the fractional derivative from (2.3), which yields

$$\mathcal{L}\{\partial_t^\alpha u(t); s\} = s^\alpha \mathcal{L}\{u(t); s\} = s^\alpha \widehat{u}(s),$$

which implies that

$$\begin{cases} (s^\alpha - \Delta)\widehat{u}(\cdot; s) = \widehat{R}(x, s) f(x) & \text{in } \Omega, \\ \widehat{u}(\cdot; s) = 0 & \text{on } \partial\Omega. \end{cases} \tag{3.9}$$

Here, $\widehat{u}(\cdot; s)$ represents the temporal Laplace transform of $u(\cdot, t)$ for $\Re s > 0$. Consequently, the time-domain solution $u(\cdot, t)$ can be retrieved by employing the inverse Laplace transform (Fourier–Mellin integral):

$$u(\cdot, t) = \frac{1}{2i\pi} \int_{s_0 - i\infty}^{s_0 + i\infty} e^{st} \widehat{u}(\cdot, s) ds, \quad s_0 > 0.$$

Under Assumption 1, we can choose H so that $\widehat{H}(x, s^{\frac{\alpha}{2}}) = \widehat{R}(x, s)$, that is,

$$H(\cdot, t) = \frac{1}{2i\pi} \int_{s_0 - i\infty}^{s_0 + i\infty} e^{st} \hat{R}(\cdot, s^{2/\alpha}) ds, \quad s_0 > 0, \tag{3.10}$$

so we construct the following wave system:

$$\begin{cases} \partial_t^2 w - \Delta w = H(x,t)f(x) & \text{in } \Omega \times (0,\infty), \\ w(x,0) = w_t(x,0) = 0 & \text{in } \Omega, \\ w(x,t) = 0 & \text{on } \partial\Omega \times (0,+\infty). \end{cases} \tag{3.11}$$

The integration path can be deformed onto the contour $\gamma(\theta_0)$ provided that R is chosen such that $\widehat{R}$ admits an analytic extension to the sector $\mathcal{S}$ (see Assumption 1).

$$H(x,t) = \frac{1}{2\pi i}\int_{\gamma(\theta_0)} R(x, s^{2/\alpha})e^{st}ds,$$

with a fixed argument $\theta_0 \in (\frac{\pi}{2}, \pi)$. The integration contour $\gamma(\theta_0)$ is defined as the union of the following three components:

1) $\{s \in \mathbb{C} : \ |s| \geq 1, \ \arg s = -\theta_0\}$;

2) $\{s \in \mathbb{C} : \ |s| = 1, \ |\arg s| \leq \theta_0\}$;

3) $\{s \in \mathbb{C} : \ |s| \geq 1, \ \arg s = \theta_0\}$.

To justify this point, we present the following supporting lemma.

Lemma 4. *Under Assumption 1 and further assuming that the Laplace transform $\widehat{R}$ allows for an analytic continuation to the sector $\{s \in \mathbb{C} \setminus \{0\} \mid |\arg s| \leq \theta_0\}$, the function H can be expressed via the following integral representation:*

$$H(x,t) = \frac{1}{2\pi i}\int_{\gamma(\theta_0)} R(x, s^{2/\alpha})e^{st}ds, \quad t > 0.$$

Proof. Given the assumptions on $R(x,t)$ and the relation $\widehat{H}(x,s) = \widehat{R}(x, s^{\frac{2}{\alpha}})$, it follows that $H(x,s)$ can be analytically extended to the sector $\{s \in \mathbb{C} \setminus \{0\} \mid |\arg s| \leq \theta_0\}$. Here, the argument θ_0 is chosen such that $\frac{\pi}{2} < \theta_0 < \pi$.

Provided no conflict occurs, the extension is likewise designated by $\widehat{H}(\cdot; s)$. We now fix $s_0 > 0$, and an application of the Fourier–Mellin formula yields

$$H(\cdot,t) = \frac{1}{2\pi i}\int_{s_0-i\infty}^{s_0+i\infty} \widehat{H}(\cdot;s)e^{st}ds, \quad t \in (0,T).$$

It follows from Jordan's lemma that the integration path can be deformed onto the contour $\gamma(\theta)$. That is,

$$H(\cdot,t) = \frac{1}{2\pi i}\int_{\gamma(\theta_0)} \widehat{H}(\cdot;s)e^{st}ds, \quad t \in (0,T). \tag{3.12}$$

By substituting $\widehat{H}(x, s^{\frac{\alpha}{2}}) = \widehat{R}(x,s)$, we finish the proof of the lemma.

From the choice of the function H, we have the relation between the Laplace transforms $\widehat{u}(x,s)$ and $\widehat{w}(x,\eta)$, that is, the following subordination principle.

Lemma 5. *Under Assumption 1, we further choose H satisfying* $\widehat{H}(x, s^{\frac{\alpha}{2}}) = \widehat{R}(x, s)$ *for all* $s > s_0$. *Then there holds* $\widehat{u}(x, s^{\frac{2}{\alpha}}) = \widehat{w}(x, s)$ *for any* $s > s_0$.

Proof. By employing the Laplace transform technique, the original problem (3.11) can be reformulated as follows.

$$\begin{cases} (\eta^2 - \Delta)\widehat{w}(\cdot; \eta) = \widehat{H}(x, \eta) f(x) & \text{in } \Omega, \\ \widehat{w}(\cdot; \eta) = 0 & \text{on } \partial\Omega. \end{cases} \tag{3.13}$$

Here, $\eta > \eta_0 > 0$. By setting $\eta^2 = s^\alpha$, it is not difficult to check that

$$\begin{cases} (s^\alpha - \Delta)\widehat{w}(\cdot; s^{\frac{\alpha}{2}}) = \widehat{H}(x, s^{\frac{\alpha}{2}}) f(x) & \text{in } \Omega, \\ \widehat{w}(\cdot; s^{\frac{\alpha}{2}}) = 0 & \text{on } \partial\Omega. \end{cases} \tag{3.14}$$

Here, $s > \eta_0^{\frac{2}{\alpha}}$. Using the assumption $\widehat{H}(x, s^{\frac{\alpha}{2}}) = \widehat{R}(x, s)$ for all $s > s_0$, it follows that

$$\begin{cases} (s^\alpha - \Delta)\widehat{w}(\cdot; s^{\frac{\alpha}{2}}) = \widehat{R}(x, s) f(x) & \text{in } \Omega, \\ \widehat{w}(\cdot; s^{\frac{\alpha}{2}}) = 0 & \text{on } \partial\Omega. \end{cases} \tag{3.15}$$

Owing to the uniqueness of the solution to the boundary value problem for elliptic equations, we obtain the identity $\widehat{w}(x, s^{\frac{\alpha}{2}}) = \widehat{u}(x, s)$. Given the observation data $u(x, t) = 0$ for $(x, t) \in \omega \times (0, \infty)$, it follows that $\widehat{w}(x, s^{\frac{\alpha}{2}}) = 0$ holds for all $x \in \omega$ and $s > \eta_0^{\frac{2}{\alpha}}$. By virtue of the uniqueness theorem for the Laplace transform, it follows immediately that $w(x, t) = 0$ throughout the domain $\omega \times (0, \infty)$.

Given the condition that $H(x, 0) \neq 0$, we invoke the established uniqueness result for the inverse source problem associated with the wave equation. Consequently, it follows that f vanishes throughout Ω. The proof is thus concluded.

3.3. Proof of the stability result

In this part, the domain is $\Omega := (0, 1)\times(0, 1)$ and R is only t-dependent. We will prove the conditional stability result of the recovering the source term by observation data in the interior domain.

We will establish the subordination principle for Eq (1.1) with the heat conduction equation and then prove the conditional stability of the inverse source problem. The initial boundary problem for the heat conduction equation we consider is as follows:

$$\begin{cases} (\partial_t - \Delta)v = H(t) f(x) & \text{in } \Omega \times (0, +\infty), \\ v(x, 0) = 0 & \text{in } \Omega, \\ v(x, t) = 0 & \text{on } \partial\Omega \times (0, +\infty), \end{cases}$$

where $x = (x_1, x_2)$. Applying the Laplace transform to (1.1) and the preceding expression yields

$$\begin{cases} (s^\alpha - \Delta)\widehat{u}(s) = \widehat{R}(s) f(x), & x \in \Omega, \\ \widehat{u}(x, s) = 0, & x \in \partial\Omega, \end{cases}$$

and

$$\begin{cases} (\eta - \Delta)\widehat{v}(\eta) = \widehat{H}(\eta) f(x) & \text{in } \Omega, \\ \widehat{v}(x, \eta) = 0 & \text{on } \partial\Omega. \end{cases}$$

Letting $s^\alpha = \eta$ and $\widehat{R}(s) = \widehat{H}(\eta)$, we get $\widehat{v}(\eta) = \widehat{u}(\eta^{\frac{1}{\alpha}})$. Thus, from the Laplace inverse transformation formula, we have

$$v(x,t) = \mathcal{L}^{-1}\{\hat{u}(x, s^{\frac{1}{\alpha}})\} = \frac{1}{2\pi i}\int_{s_0-i\infty}^{s_0+i\infty} \widehat{u}(x, s^{\frac{1}{\alpha}})e^{st}ds. \tag{3.16}$$

From the Cauchy integral theorem and noting that $\frac{1}{2} < \frac{1}{\alpha} < 1$ $(1 < \alpha < 2)$, we can change the above integration path to

$$v(x,t) = \frac{1}{2\pi i}\int_{\gamma} \widehat{u}(x, s^{\frac{1}{\alpha}})e^{st}ds, \tag{3.17}$$

where γ is defined as follows: $\gamma = \gamma_+ \cup \gamma_- \cup \gamma_\varepsilon$, where

$$\gamma_\pm := \{\arg z = \pm\theta_0,\ |z| \geq \varepsilon\},$$

$$\gamma_\varepsilon := \{|z| = \varepsilon,\ |\arg z| \leq \theta_0\},$$

and θ_0 is between $\pi/2$ and π, and $\alpha\pi/2 < \theta_0 < \pi$.

Next, we will use the observation data

$$u(x,t),\ (x,t) \in \omega \times (0,T),\ \textit{where } \omega \subset \Omega \textit{ and boundary } \{(x_1,0)\} \subset \partial\omega$$

to prove the conditional stability of the inverse source problem.

Proof of Theorem 2. We have

$$\|f\|_{L^2(\Omega)} \leq C|\log \|\partial_{x_2} v(x_1,0,t)\|_{H^1(0,T;L^2(0,1))}|^{-\beta}, \quad \beta > 0,$$

which, combined with the trace theorem, further yields

$$\|f\|_{L^2(\Omega)} \leq C|\log \|v(x_1,x_2,t)\|_{H^1(0,T;H^2(\omega))}|^{-\beta}.$$

On the other hand, noting (3.16), we directly take a $\|\cdot\|_{H^1(0,T;H^2(\omega))}$ norm on both sides of (3.16) to get

$$\|v\|_{H^1(0,T;H^2(\omega)} \leq C\left\|\mathcal{L}^{-1}\{\widehat{u}(\cdot, s^{\frac{1}{\alpha}}); t\}\right\|_{H^1(0,T;H^2(\omega))},$$

and thus,

$$\|f\|_{L^2(\Omega)} \leq C|\log \|\mathcal{L}^{-1}\{\widehat{u}(\cdot, s^{\frac{1}{\alpha}}); t\}\|_{H^1(0,T;H^2(\omega))}|^{-\beta}.$$

The stability result is proved. We complete the proof of the theorem.

4. The framework of the L-PINNs

4.1. The general PINNs method

We begin by considering the general framework for data-driven modeling on a spatial domain $\Omega \subset \mathbb{R}^d$. The governing dynamics are described by a time-dependent partial differential equation of the form

$$u_t + \mathcal{N}[u;\lambda] = 0, \quad x \in \Omega,\ t \in [0,T], \tag{4.1}$$

where $u(x,t)$ represents the system state, and $\mathcal{N}[\cdot;\lambda]$ signifies a nonlinear spatial operator governed by a set of parameters λ.

PINNs methods distinguish themselves from conventional neural network architectures by embedding the laws and principles of physics, represented by partial differential equations such as $f := u_t + \mathcal{N}[u; \lambda]$ into their framework. This integration of domain-specific knowledge directly into the loss function transforms the training process into an optimization problem, allowing the data to approximate solutions efficiently and accurately. By merging the data-driven capabilities of deep learning with the knowledge-driven rigor of traditional numerical methods, PINNs offer a unique hybrid approach. To obtain the optimal shared parameters θ, we minimize the mean squared error (MSE) loss as follows.

$$Loss = Loss_u + Loss_f, \tag{4.2}$$

where

$$Loss_u = \frac{1}{N_u}\sum_{i=1}^{N_u}|u_{NN}(x_u^i, t_u^i) - u^i|^2, \tag{4.3}$$

and

$$Loss_f = \frac{1}{N_f}\sum_{i=1}^{N_f}|f_{NN}(x_f^i, t_f^i)|^2. \tag{4.4}$$

Here, $\{u^i\}_{i=1}^{N_u}$ denotes the initial and boundary training data on the collocation points $\{x_u^i, t_u^i\}_{i=1}^{N_u}$, and $\{x_f^i, t_f^i\}$ specifies the collocation points for f. The network structure of PINNs is shown in Figure 1.

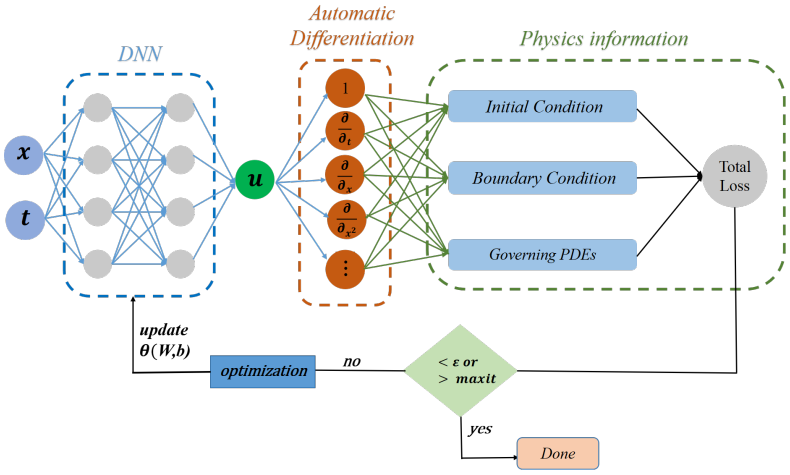

Figure 1. Schematic structure of physics-informed neural networks.

4.2. Laplace-based PINNs

The computation of fractional derivatives, which entails integrating functions alongside integer-order derivatives, inherently requires advanced numerical or integral methods. This complexity poses a considerable challenge for the PINNs in solving fractional partial differential equations. Caputo derivatives, a category of fractional-order derivatives, are widely employed to characterize nonlinear and nonlocal dynamical systems. Unlike their integer-order counterparts, Caputo derivatives deviate from the classical chain rule, hindering the straightforward application of automatic differentiation

techniques in the PINNs method. This presents challenges in embedding physical constraints during the neural network training process. Therefore, it is crucial to investigate novel neural network methodologies that address the limitations of PINNs, specifically regarding numerical computation complexity, integration of physical constraints, and network architecture design.

To address the aforementioned challenges, we propose the Laplace-based physics-informed neural network (L-PINNs) method for solving the fractional nonlocal diffusion-wave equation (1.1). This novel approach enhances the traditional PINNs method by incorporating Laplace transforms. The key innovation of L-PINNs lies in simplifying the computation of time-fractional derivatives via Laplace transforms, thereby reducing both computational costs and the complexity of embedding physical constraints into neural networks. The network is structured to represent both the solution of the equation and the unknown coefficients in the Laplace domain. Subsequently, numerical inversion is employed to obtain the predicted solutions and coefficients. In the following sections, we provide a detailed analysis of the approach process for the inverse problem of time-fractional partial differential equations using this new method.

4.2.1. Laplace transform

The Laplace transform is a potent mathematical tool widely employed in engineering and physics for the analysis of linear time-invariant systems. Consider a function $f(t)$ dependent on the time variable $t \in [0, +\infty)$. If the integral

$$F(s) = \mathcal{L}\{f; s\} = \int_0^{+\infty} f(t)e^{-st}dt \tag{4.5}$$

converges in a region of the complex plane for the complex variable $s \in \mathbb{C}$, the complex variable function $F(s)$ is said to be the Laplace transform of the real variable function $f(t)$. $F(s)$ and $f(t)$ are referred to as the image function and the original function, respectively. Furthermore, the Laplace transform is a linear operator. This implies that for any constants a, b and functions $f(t)$, $g(t)$, the following property holds:

$$\mathcal{L}\{af + bg; s\} = a\mathcal{L}\{f, s\} + b\mathcal{L}\{g; s\}. \tag{4.6}$$

Particularly, the Laplace transform of the time-fractional Caputo derivative $\partial_t^\alpha f(t)$ can be written as

$$\mathcal{L}\{\partial_t^\alpha f(t); s\} = s^\alpha F(s) - s^{\alpha-1} f(0), \quad t \in [0, +\infty),\ \alpha \in (0, 1). \tag{4.7}$$

Based on the above preparatory knowledge and the key properties of Laplace transform, we perform the Laplace transform on both sides of the equation (1.1), which ultimately results in

$$\begin{cases} s^\alpha \widehat{u}(x, s) - \Delta\widehat{u}(x, s) = s^{\alpha-1}u_0(x) + \widehat{R}(x, s)f(x), & x \in \Omega,\ s \in \mathbb{C}, \\ \widehat{u}(x, s) = 0, & x \in \partial\Omega,\ s \in \mathbb{C}, \end{cases} \tag{4.8}$$

where $\widehat{u}(x, s) = \mathcal{L}\{u; s\}$, $\widehat{R}(x, s) = \mathcal{L}\{R; s\}$. The problem has clearly been reduced to solving an integer-order partial differential equation, which can be effectively addressed using the PINNs method.

4.2.2. The structure of L-PINNs

Given the initial value $u_0(x)$, the order α, and $R(x,t)$ in Eq (1.1), we aim to invert both the coefficient $f(x)$ and the exact solution $u(x,t)$. To infer the entire spatiotemporal solution u and the f, we approach the corresponding Laplace-transformed solution and the coefficient by using two deep neural networks, denoted as $\widehat{u}_{NN}(x,s)$ and $\widehat{f}_{NN}(x,s)$, respectively. By combining these networks with the physical constraints, we construct the Laplace-based physics-informed neural network $L_{NN}(x,s)$. The shared parameters of these networks are optimized by minimizing the mean square error loss,

$$Loss = w_{eq}L_{eq}(\theta_1,\theta_2) + w_{bd}L_{bd}(\theta_1) + w_{obs}L_{obs}(\theta_1) + w_{prior}L_{prior}(\theta_2), \tag{4.9}$$

where

$$\begin{cases} L_{eq} = \dfrac{1}{N_{eq}}\displaystyle\sum_{i=1}^{N_{eq}} |L_{NN}(x_{in}^i, s_{in}^i)|^2, \\ L_{bd} = \dfrac{1}{N_{bd}}\displaystyle\sum_{i=1}^{N_{bd}} |\widehat{u}_{NN}(x_{bd}, s_{bd}^i)|^2, \\ L_{obs} = \dfrac{1}{N_{obs}}\displaystyle\sum_{i=1}^{N_{obs}} |\widehat{u}_{NN}(x_{obs}^i, s_{obs}^i) - \widehat{u}^i|^2, \\ L_{prior} = \dfrac{1}{N_{prior}}\displaystyle\sum_{i=1}^{N_{prior}} |\dfrac{1}{s_{in}^i} f^i - \widehat{f}_{NN}(x_{in}^i, s_{in}^i)|^2, \end{cases} \tag{4.10}$$

and

$$\begin{aligned} L_{NN}(x,s) = {} & s^{\alpha}\widehat{u}_{NN}(x,s) - \Delta\widehat{u}_{NN}(x,s) - s^{\alpha-1}u_0(x) \\ & - \widehat{R}(x,s)\widehat{f}_{NN}(x,s)s. \end{aligned} \tag{4.11}$$

w_{eq}, w_{bd}, w_{obs}, w_{prior} are loss weights and θ_1 and θ_2 are trainable parameters for networks $\widehat{u}_{NN}(x,s)$ and $\widehat{f}_{NN}(x,s)$, respectively. Moreover, $\{x_{bd}, s_{bd}^i\}_{i=1}^{N_{bd}}$ denotes the boundary training points, and $\{x_{obs}^i, s_{obs}^i\}_{i=1}^{N_{obs}}$ are the training data for observations on $\widehat{u}$. $\{x_{in}^i, s_{in}^i\}_{i=1}^{N_{eq}}(N_{eq} = N_{prior})$ in L_{eq} and L_{prior} are the collocation points on $L_{NN}(x,s)$. The network architecture of L-PINNs is shown in Figure 2.

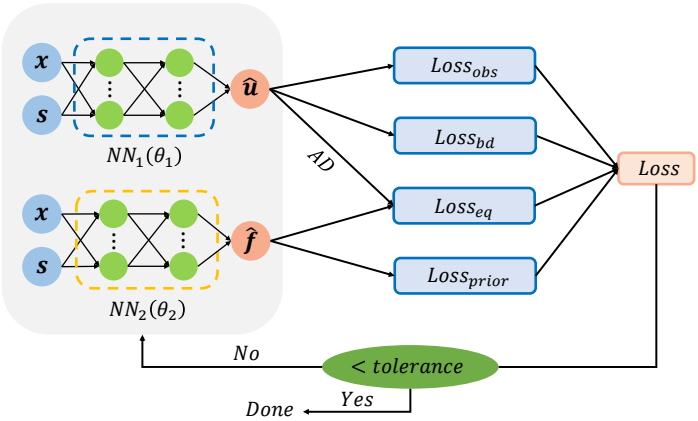

Figure 2. Schematic structure of physics-informed neural networks in the Laplace domain: the network NN_1 with parameter θ_1 approximates $\widehat{u}$, and the network NN_2 with parameter θ_2 approximates $\widehat{f}$, where AD denotes automatic differentiation.

Remark 1. *We could have defined the loss L_{prior} in the real domain*

$$L_{prior} = \frac{1}{N_{prior}} \sum_{i=1}^{N_{prior}} |f^i - f_{NN}(x_{in}^i)|^2, \tag{4.12}$$

which would have resulted in a more streamlined network structure, but after experimentation, we found that defining the individual loss terms uniformly in the Laplace domain gave more accurate results. Moreover, we ensure that the total number of training points is not excessive by designing the training data of L_{eq} to be the same as L_{prior}.

Note that the numerical $\widehat{u}_{NN}(x, s)$ obtained by minimizing the loss function (4.9) are the approximation to Eq (4.8). In order to convert the $\widehat{u}_{NN}(x, s)$ in the Laplace space domain into a solution $u(x, t)$ of the original problem (1.1), we explore the numerical inverse Laplace transform (NILT) method. The inverse Laplace transform is the process of obtaining the original function from the inversion of the image function. Various numerical inversion algorithms for Laplace transforms have been proposed by researchers. In this paper, we have chosen to use the Gaver-Stehfest algorithm [39], which is distinguished by the fact that the summation weights and nodes do not depend on the complex numbers.

By applying the Gaver–Stehfest algorithm, we find that the transformation formula between the solution $\widehat{u}(x, s)$ in the Laplace space domain and the solution $u(x, t)$ of the original problem at a specific time t can be expressed as [40]

$$u(x, t) = \frac{\ln 2}{t} \sum_{i=1}^{M} \mu_i \widehat{u}(x, \frac{\ln 2}{t} i) \tag{4.13}$$

and

$$\mu_i = (-1)^{\frac{M}{2}+i} \sum_{k=[\frac{i+1}{2}]}^{\min(i,\frac{M}{2})} \frac{k^{\frac{M}{2}}(2k)!}{(\frac{M}{2}-k)!k!(k-1)!(i-k)!(2k-i)!}, \tag{4.14}$$

where M is an even number, and $[(i + 1)/2]$ denotes the largest integer not exceeding the real number $(i + 1)/2$. From Eq (4.13), we are able to find that $u(x, t)$ is expressed as a linear combination of $\{\widehat{u}(x, s_i = i \ln 2/t)\}_{i=1}^{M}$, where the range of values of s_i $(i = 1, \ldots, M)$ will be elucidated in numerical experiments.

The lower bound $s_{\min} = \ln 2/T$ ensures that the network captures the physics at the maximum observation time T. The upper bound $s_{\max} = M \ln 2/t_1$ covers the high-frequency components required to reconstruct the solution at the initial stage t_1. By training the L-PINN within this specific s-range, we ensure that the neural network "sees" all the necessary support points in the Laplace domain required for accurate time-domain reconstruction.

5. Numerical validations

We now proceed to validate the performance and robustness of the proposed L-PINNs framework in tackling inverse problems for time-fractional differential equations. Our assessment covers both one-dimensional and two-dimensional benchmarks. To quantitatively evaluate the reconstruction quality, we employ relative L^2 error metrics for the terminal solution $u(\cdot, T)$ and the identified source term $f(\cdot)$,

defined respectively as

$$Error_u(T) = \frac{\| u(\cdot, T) - u_{NN}(\cdot, T) \|_2}{\| u(\cdot, T) \|_2}, \quad Error_f = \frac{\| f - fNN \|_2}{\| f \|_2}. \tag{5.1}$$

Here, the subscript NN denotes the neural network approximation, and variables without subscripts represent the exact reference solutions.

During the training process, we choose networks with the Swish activation function. Swish is computationally as efficient as ReLU and exhibits better performance than ReLU on deeper models. Considering the advantages of the Adam algorithm in nonconvex optimisation problems, we choose it to iteratively update the neural network parameters based on the training data. In particular, we choose $\{u_{NN}(x_i, T)\}_{i=1}^{101}$ and $\{f_{NN}(x_i)\}_{i=1}^{101}$ as the test set for calculating the relative error, which are not involved in the learning process of the network parameters and only evaluate the final model after the training is completed. Here, $\{x_i\}_{i=1}^{101}$ are equidistant points on the spatial domain.

Example 5.1. *One-dimensional problem*

Consider the time-fractional differential equation

$$\begin{cases} \partial_t^\alpha u - \Delta u = R(x,t)f(x), & (x,t) \in \Omega \times (0,1], \\ u(x,0) = u_t(x,0) = 0, & x \in \Omega, \\ u(x,t) = 0, & (x,t) \in \partial\Omega \times (0,1], \end{cases} \tag{5.2}$$

where

$$\begin{cases} R(x,t) = \dfrac{E_{\alpha,1}(-t^\alpha)(\varphi + \Delta\varphi) - \Delta\varphi}{x+1}, \\ \varphi(x) = x^2 - x, \\ f(x) = x + 1. \end{cases} \tag{5.3}$$

Here, $\Omega = [0,1]$, with the exact solution of this equation given by $u(x,t) = [1 - E_{\alpha,1}(-t^\alpha)]\varphi(x)$, where $E_{\alpha,1}(-t^\alpha)$, is the Mittag-Lefflerr function in two-parameter form, and its Laplace transform formula can be simply defined as $\mathcal{L}\{E_{\alpha,1}(-t^\alpha); s\} = s^{\alpha-1}/(s^\alpha + 1)$.

Applying the Laplace transform to both sides of the initial fractional order Eq (5.2) with respect to the time variable yields the following equation:

$$\begin{cases} s^\alpha \widehat{u} - \widehat{u}_{xx} = s^{\alpha-1}u(x,0) + \dfrac{\frac{s^{\alpha-1}}{s^\alpha+1}(\varphi + \Delta\varphi) - \frac{\Delta\varphi}{s}}{x+1}\widehat{f}(x,s)s, & x \in \Omega,\ s \in \mathbb{C}, \\ \widehat{u}(x,s) = 0, & x \in \partial\Omega,\ s \in \mathbb{C}. \end{cases} \tag{5.4}$$

The parameters (θ_1, θ_2) of the approximate solution $\widehat{u}_{NN}(x; s; \theta_1)$ and the approximate source $\widehat{f}_{NN}(x; s; \theta_2)$ are optimized by minimizing the following loss function in (4.9),

$$\begin{aligned} &(\theta_1^*, \theta_2^*) = \arg\min Loss \\ &= w_{eq}L_{eq}(\theta_1, \theta_2) + w_{bd}L_{bd}(\theta_1) + w_{obs}L_{obs}(\theta_1) + w_{prior}L_{prior}(\theta_2). \end{aligned} \tag{5.5}$$

We set $M = 4$ in the Gaver–Stehfest algorithm (4.13) and sample the training points s within the interval $S = [s_{min}, s_{max}]$, where $s_{min} = \ln 2/T$, $s_{max} = M \ln 2/t_1$, and $t_1 = 0.01$.

In this experiment, we employ $N_{eq} = 3000$ collocation points on loss $L_{eq}(\theta)$ and $N_{bd} = 1200$ on the boundary loss $L_{bd}(\theta)$, respectively. The weights assigned to these two loss terms are $w_{eq} = 2$ and $w_{bd} = 2000$. Specifically, the additional measurements are given by

$$h(x,t) = u(x,t) + \epsilon u(x,t)$$

with a random sampling of $N_{obs} = 5000$ observations and $\epsilon = 0.001$ within the specified region $x \in [0, 0.5]$.

To infer the solution $\widehat{u}(x,s)$, we employ a neural network consisting of five hidden layers, each with 256 neurons. We represent the unknown coefficient $\widehat{f}(x,s)$ using a fully connected neural network with four hidden layers, and each contains 64 neurons. During training, the weight coefficients of the loss function are fixed at $w_{obs} = 1000$ and $w_{prior} = 1000$. $N_{obs} = 5000$ and $N_{prior} = 3000$ represent the batch sizes of the observation points corresponding to the measurement data and the known points for $f(x)$, respectively.

In this example, we have the tests with $\alpha = 1.2$ and $\alpha = 1.4$ to validate the efficiency and accuracy of the L-PINNs method. After 20,000 epochs of training, the relative errors and simulation results are presented in Table 1 and Figure 3. These findings demonstrate that the L-PINNs method effectively reconstructs the source function f and predicts the solution u simultaneously when additional measurement data is included.

Table 1. Comparison of relative errors and training runtime for 1D Example 5.3 ($W_{eq} = 2$, iter = 20, 000).

Method	α	u relative error	f relative error	Runtime (s)
L-PINNs	1.2	0.044137	0.004039	315
	1.4	0.036985	0.039882	315
f-PINNs	1.2	0.048612	0.063517	528
	1.4	0.046127	0.082365	528

To rigorously assess the capabilities of L-PINNs, we benchmark the proposed framework against standard fractional physics-informed neural networks (f-PINNs). In the f-PINN implementation, the temporal fractional operator is handled using the finite difference method. Specifically, we incorporate the $L2$ discretization scheme proposed by Li [41] into the loss function to resolve the time-fractional inverse problem. The discrete approximation of the Caputo derivative at node t_n is given by

$$\left[C\mathrm{D}^{\alpha}_{0,t} f(t)\right]_{t=t_n} = \sum_{k=-1}^{n} W_k f(t_{n-k}) + O(\Delta t^{3-\alpha}), \quad 1 < \alpha < 2,$$

where the convolution coefficients W_k are defined as

$$W_k = \frac{\Delta t^{-\alpha}}{\Gamma(3-\alpha)} \begin{cases} 1 & k = -1, \\ 2^{2-\alpha} - 3 & k = 0, \\ (k+2)^{2-\alpha} - 3(k+1)^{2-\alpha} + 3k^{2-\alpha} - (k-1)^{2-\alpha} & 1 \le k \le n-2, \\ -2n^{2-\alpha} + 3(n-1)^{2-\alpha} - (n-2)^{2-\alpha} & k = n-1, \\ n^{2-\alpha} - (n-1)^{2-\alpha} & k = n. \end{cases}$$

The relative errors and simulation results are presented in Table 1 and Figure 4. Experimental results show that L-PINNs achieve slightly better performance than f-PINNs for the inverse reconstruction of the source term f. Furthermore, for 1D Example 5.3 (20,000 epochs), L-PINNs completed training in approximately 315 seconds, whereas f-PINNs required 528 seconds, indicating that L-PINNs achieved a 40% reduction in total training time.

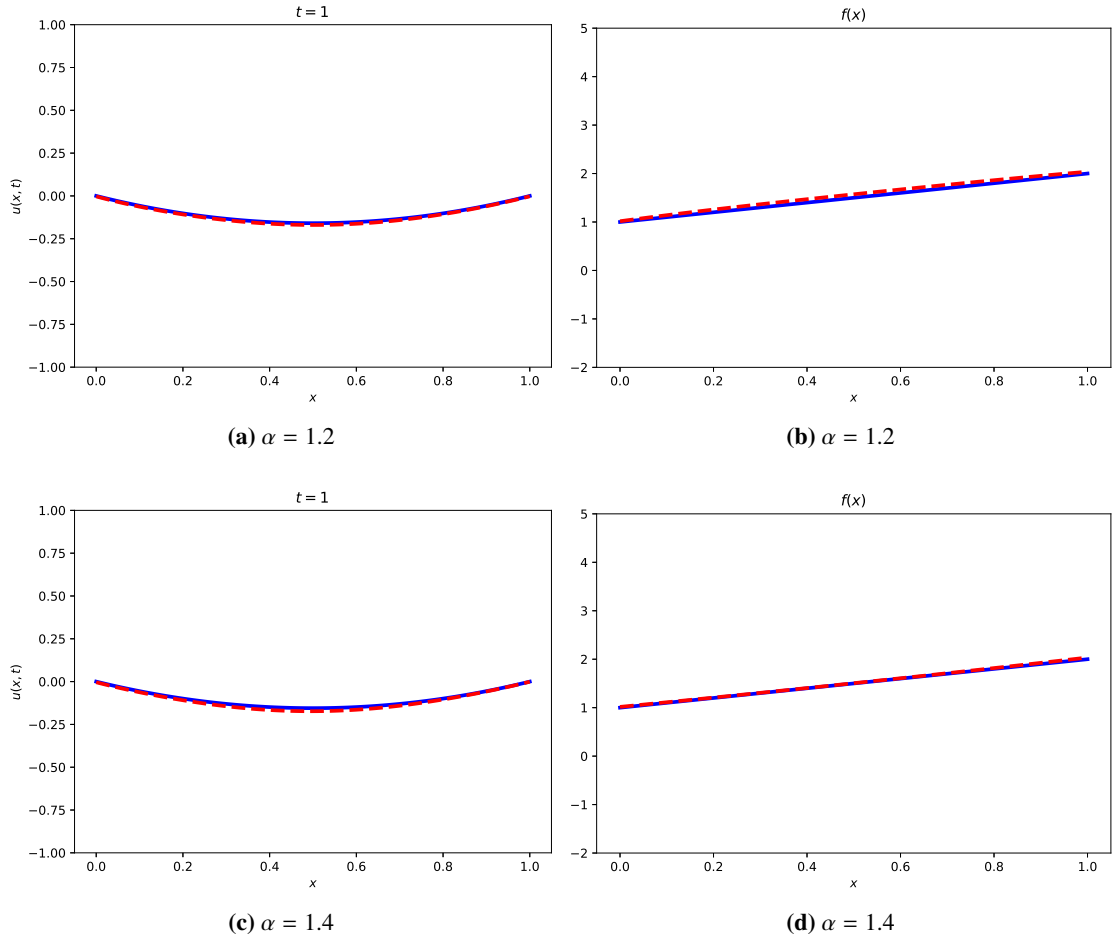

(a) $\alpha = 1.2$ **(b)** $\alpha = 1.2$

(c) $\alpha = 1.4$ **(d)** $\alpha = 1.4$

Figure 3. The exact solutions (blue) and numerical approximations (red) from L-PINNs for u and f at the final moment $T = 1$.

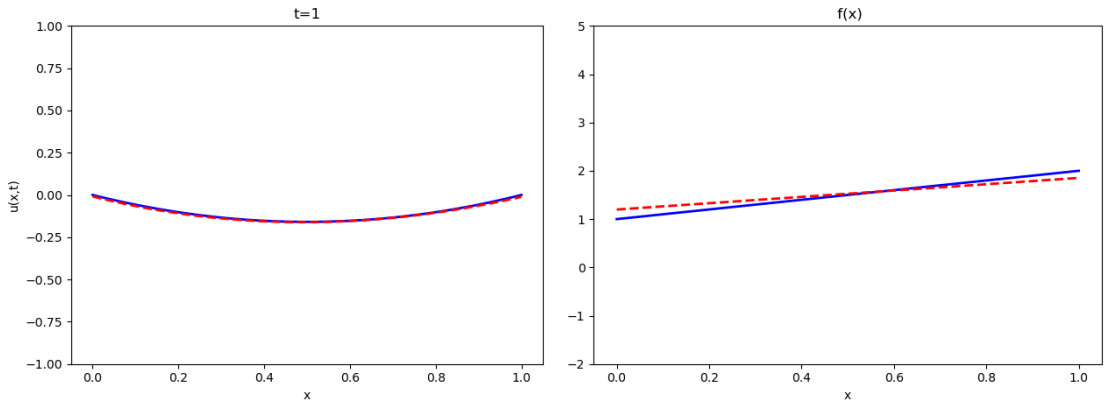

(a) $\alpha = 1.2$ **(b)** $\alpha = 1.2$

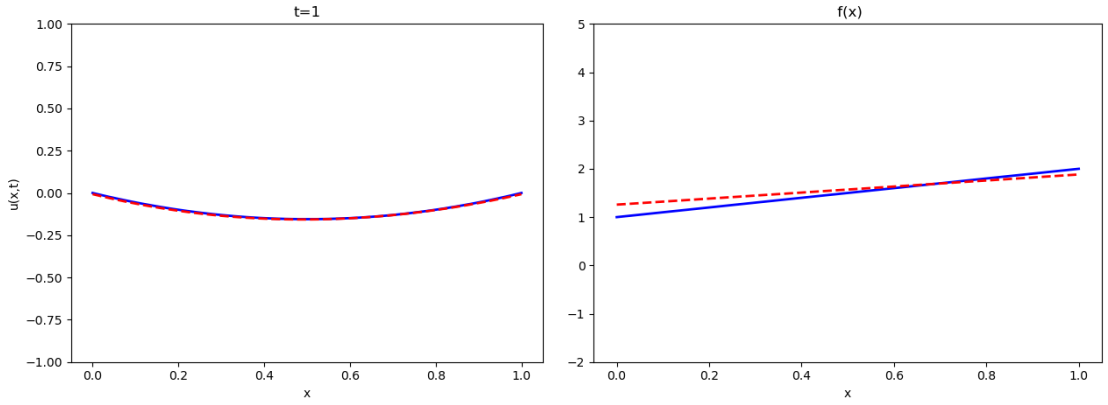

(c) $\alpha = 1.4$ **(d)** $\alpha = 1.4$

Figure 4. The exact solutions (blue) and numerical approximations (red) from f-PINNs for u and f at the final moment $T = 1$.

Example 5.2. *Two-dimensional problem*

In this part, we study the performance of the L-PINNs method to solve an inverse problem of the two-dimensional time-fractional differential equation

$$\begin{cases} \partial_t^\alpha u - \Delta u = R(x,y,t)f(x), & (x,y,t) \in \Omega \times (0,1], \\ u(x,y,0) = u_t(x,y,0) = 0, & (x,y) \in \Omega, \\ u(x,y,t) = 0, & (x,y,t) \in \partial\Omega \times (0,1], \end{cases} \tag{5.6}$$

where

$$\begin{cases} R(x,y,t) = \dfrac{E_{\alpha,1}(-t^\alpha)(\varphi + \Delta\varphi) - \Delta\varphi}{\sin x + 2}, \\ \varphi(x,y) = \sin \pi x \sin \pi y. \end{cases} \tag{5.7}$$

Here, we consider the source function $f(x) = \sin(x) + 2$ and corresponding solution $u(x,y,t) = [1 - E_{\alpha,1}(-t^\alpha)] \sin(\pi x) \sin(\pi y)$. The spatial domain is $[0,1] \times [0,1]$. In this part, we consider the inverse problem of identifying the source function f and solution u from additional measurements of u, given

that the initial values, $R(x, y, t)$ and fractional order α are known. Specifically, the extra measurements are given by

$$h(x, y, t) = \partial_x u(0, y, t) + \epsilon \partial_x u(0, y, t),$$

where $\partial_x u(0, y, t) = [1 - E_{\alpha,1}(-t^\alpha)]\pi \sin(\pi y)$.

Simultaneous Laplace transform on both sides of the Eq (5.6) with respect to time t give

$$\begin{cases} s^\alpha \widehat{u} - \widehat{u}_{xx} - \widehat{u}_{yy} = s^{\alpha-1} u(x, y, 0) + \dfrac{\frac{s^{\alpha-1}}{s^\alpha+1}(\varphi + \Delta\varphi) - \frac{\Delta\varphi}{s}}{\sin x + 2} \widehat{f}(x, s)s, \\ (x, y) \in \Omega, \ s \in \mathbb{C}, \\ \widehat{u}(x, y, s) = 0, \quad (x, y) \in \partial\Omega, \ s \in \mathbb{C}. \end{cases} \tag{5.8}$$

To infer the complete spatiotemporal solution u of the equation and the source f, we utilize a neural network architecture consisting of a 5-layer network with 256 neurons per layer for $\widehat{u}(x, y, s)$ and a 4-layer network with 64 neurons per layer for $\widehat{f}(x, s)$. Importantly, it should be noted that the input s of the neural network herein adopts the same values as in Example 5.3.

We use the same technique (5.5) in Example 5.3 to approximate the parameters (θ_1, θ_2) of the approximate solution $\widehat{u}_{NN}(x; s; \theta_1)$ and the approximate source $\widehat{f}_{NN}(x; s; \theta_2)$. Then, we apply $N_{eq} = 3000$ randomly sampled collocation points for enforcing equation (5.8) on $L_{eq}(\theta)$ and $N_{bd} = 1200 \times 4$ randomly sampled boundary points on $L_{bd}(\theta)$ in the Laplace domain. The additional measurements for this example consist of $N_{obs} = 5000$ data points satisfying $h(x, y, t)$. It is worth noting that the weight coefficients of the loss function are $w_{eq} = 1$, $w_{obs} = 100$, $w_{bd} = 2000$, and $w_{prior} = 1000$ during the training process. Finally, after 1.5×10^5 iterations, our experimental results for different α are summarized in Table 2 and Figures 5 and 6. We can find that the L-PINNs method can achieve the higher accuracy for the inverse source problem in two-dimensional time-fractional differential equations.

Table 2. Comparison of relative errors and training runtime for 2D Example 5.2 (iter = 150, 000).

Method	α	u relative error	f relative error	Runtime (s)
L-PINNs	1.2	0.066460	0.013499	4635
	1.4	0.114942	0.002631	4632
	1.6	0.241109	0.007383	4635
	1.8	0.419585	0.001719	4635
f-PINNs	1.2	0.043156	0.016234	8421
	1.4	0.012865	0.017233	8422
	1.6	0.059821	0.016582	8420
	1.8	0.072152	0.012683	8420

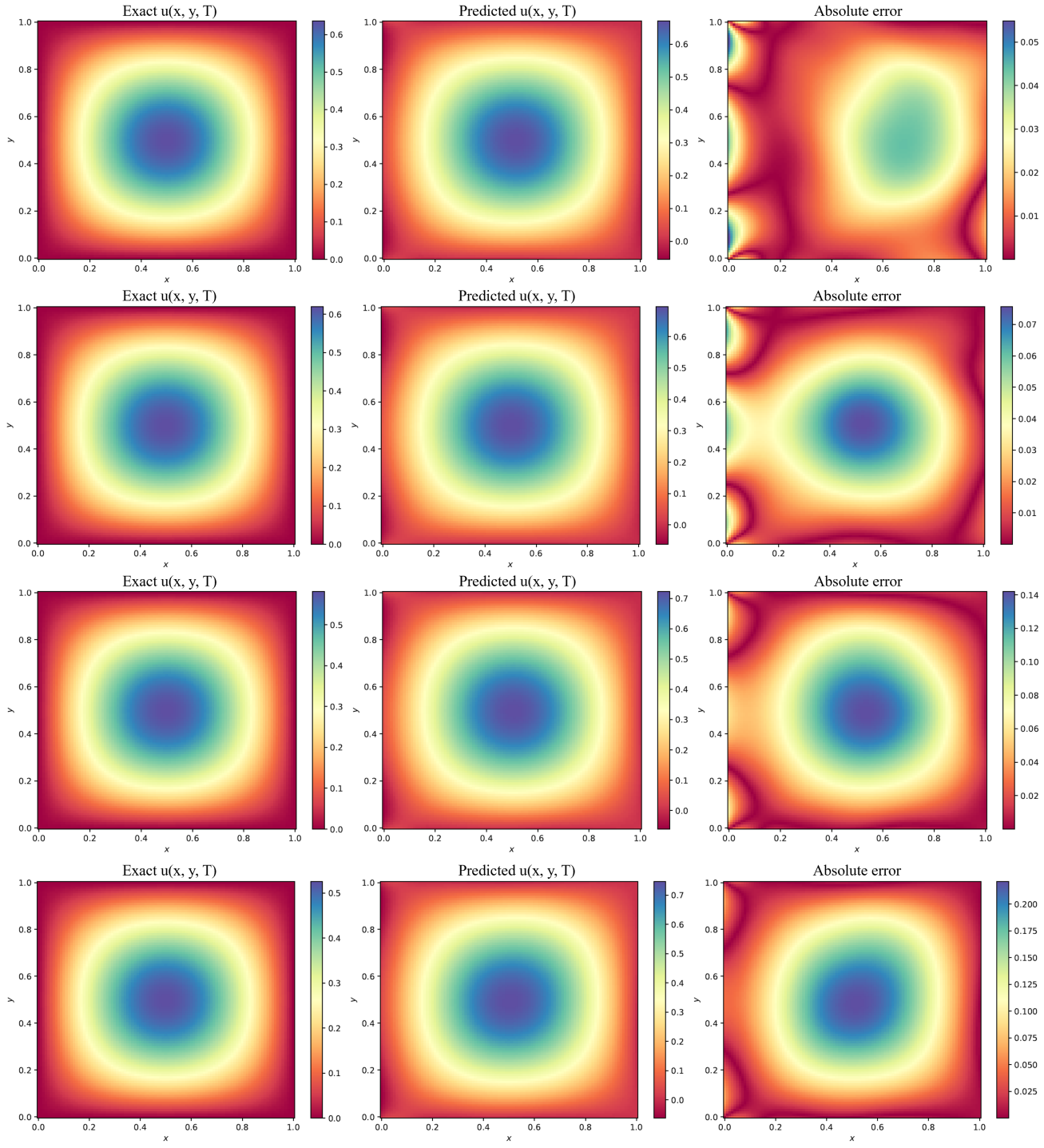

Figure 5. The exact solution $u(x, y, T)$, the predicted solution $u_{NN}(x, y, T)$ from L-PINNs, and the absolute error $|u(x, y, T) - u_{NN}(x, y, T)|$ at the moment $T = 1$ for different $\alpha = 1.2$, $\alpha = 1.4$, $\alpha = 1.6$, and $\alpha = 1.8$ (from top to bottom).

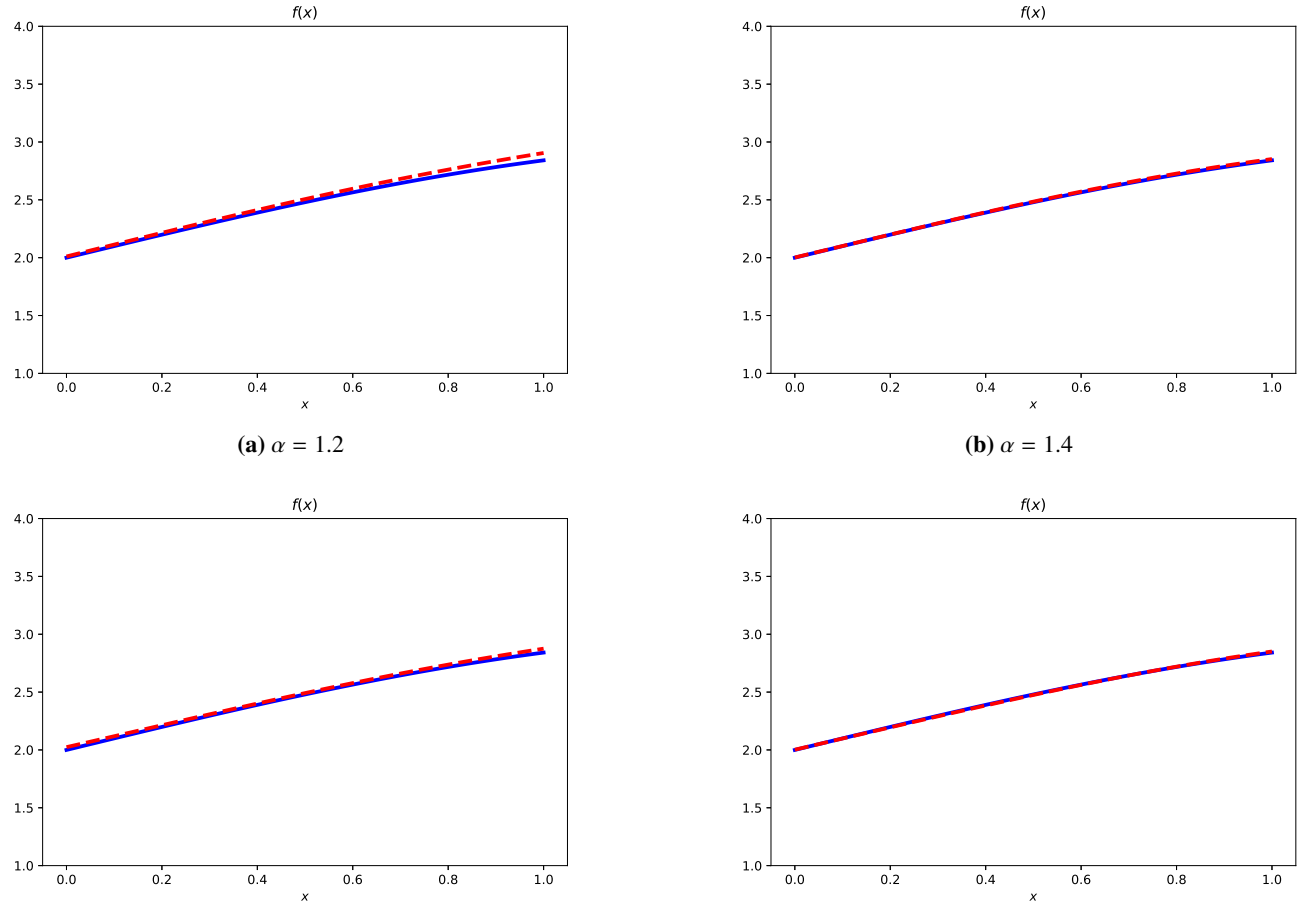

(a) $\alpha = 1.2$ **(b)** $\alpha = 1.4$

(c) $\alpha = 1.6$ **(d)** $\alpha = 1.8$

Figure 6. The reconstruction from L-PINNs (red) and the exact function (blue) for the source f with different α.

Just like with the 1D case, we also conducted a comparative experiment using f-PINNs for the 2D case. the relative errors and simulation results are presented in Table 2 and Figures 7 and 8. Similarly, we can generally draw the same conclusion as in the 1D case: the L-PINNs method outperforms f-PINNs in reconstructing the source term f. Furthermore, for 2D Example 5.2, L-PINNs completed training in approximately 4635 seconds, whereas f-PINNs required about 8421 seconds, indicating that L-PINNs achieved a 45% reduction in total training time.

We also find that although the error reduction from our method compared to f-PINNs may appear modest in terms of absolute magnitude, the primary advantage of L-PINNs lies in computational robustness rather than just lower error values. Standard f-PINNs rely on numerical discretization (L2 scheme) of the fractional operator, which introduces systematic discretization errors. L-PINNs eliminate this discretization by solving the problem in the Laplace domain, which provides a more consistent physical constraint across the entire domain. Furthermore, L-PINNs demonstrate superior performance in reconstructing the unknown source term $f(x)$, which is generally more challenging than predicting the state $u(x, t)$.

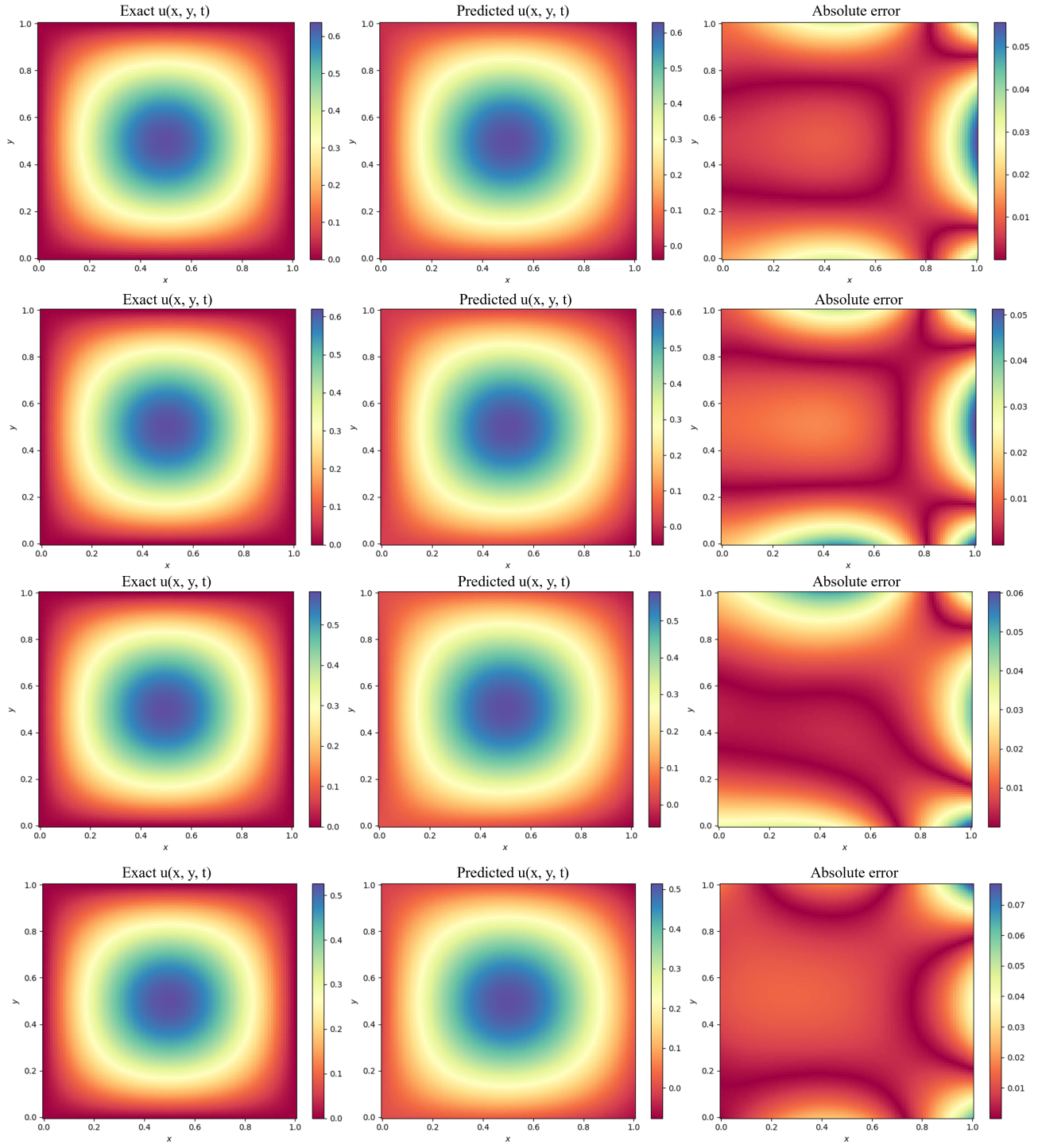

Figure 7. The exact solution $u(x, y, t)$, the predicted solution $u_{NN}(x, y, t)$ from f-PINNs, and the absolute error $|u(x, y, t) - u_{NN}(x, y, t)|$ at the moment $t = 1$ for different $\alpha = 1.2$, $\alpha = 1.4$, $\alpha = 1.6$, and $\alpha = 1.8$ (from top to bottom).

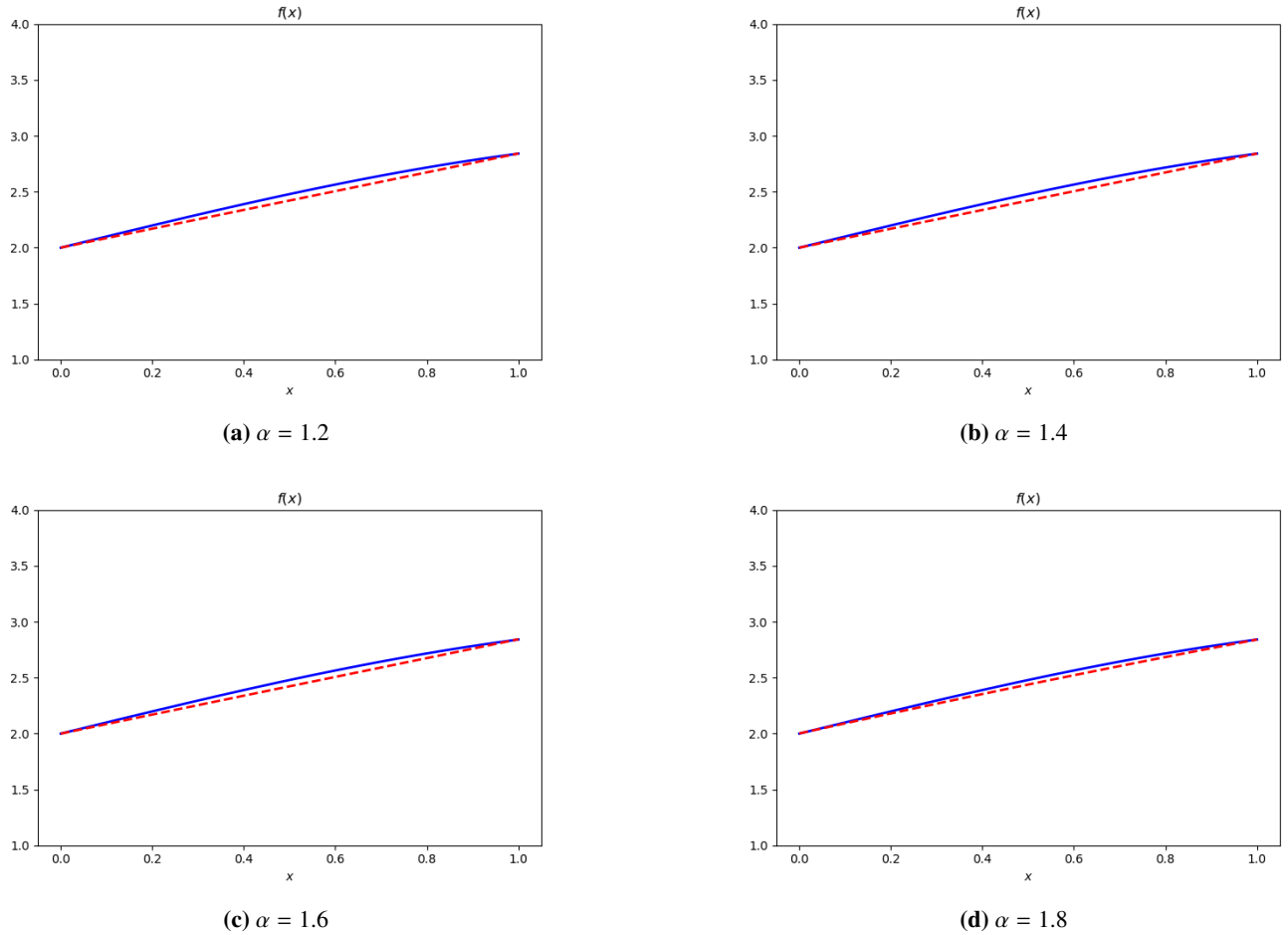

(a) $\alpha = 1.2$ **(b)** $\alpha = 1.4$

(c) $\alpha = 1.6$ **(d)** $\alpha = 1.8$

Figure 8. The reconstruction form f-PINNs (red) and the exact function (blue) for the source f with different α.

Example 5.3. *Sensitivity analysis*

To further evaluate the robustness of the L-PINNs framework, we investigate the sensitivity of the reconstruction accuracy to the parameter M with the Gaver–Stehfest algorithm. We conduct tests on both 1D and 2D benchmarks across different fractional orders $\alpha \in (1, 2)$. As defined in (5.1), we monitor the fluctuations of $Error_u$ and $Error_f$ when M is set to 4, 6, and 8.

As summarized in Tables 3 and 4, we find $M = 4$ to be a robust balance point, providing sufficient accuracy for both 1D and 2D inverse source problems while maintaining numerical stability across various α values. For a fixed α, increasing M from 4 to 6 typically maintains or slightly improves the accuracy. However, as M reaches 8, the errors exhibit a noticeable upward trend across all tested α values. This phenomenon can be attributed to the nature of the Gaver–Stehfest coefficients μ_i. As M increases, these coefficients grow exponentially in magnitude and alternate in sign (e.g., for $M = 8$, $|\mu_i|$ can exceed 1.8×10^4). Consequently, any small approximation error from the neural network in the Laplace domain is significantly amplified, leading to numerical instability in the time-domain reconstruction. These results justify our choice of $M = 4$ as an optimal balance between sampling density and numerical robustness.

Table 3. Sensitivity results for 1D Example 5.1 with different M and α.

α	Error Type	$M = 4$ (Baseline)	$M = 6$	$M = 8$
1.2	*u relative error*	0.044137	0.045218	0.071825
	f relative error	0.004039	0.004851	0.012534
1.4	*u relative error*	0.036985	0.038512	0.064219
	f relative error	0.039882	0.041235	0.089407

Table 4. Sensitivity results for 2D Example 5.2 with different M and α.

α	Error Type	$M = 4$ (Baseline)	$M = 6$	$M = 8$
1.2	*u relative error*	0.066460	0.068125	0.105432
	f relative error	0.013499	0.014210	0.032845
1.6	*u relative error*	0.241109	0.245518	0.312047
	f relative error	0.007383	0.008105	0.019562

6. Conclusions

This article presented a novel framework combining Laplace transforms with physics-informed neural networks (L-PINNs) to reconstruct unknown source terms in nonlocal diffusion-wave equations. On the theoretical front, we rigorously established the time-analyticity of the forward solution by exploiting Fourier expansions and the asymptotic properties of Mittag-Leffler functions. Furthermore, the subordination principle linking parabolic and hyperbolic regimes was elucidated through the lens of the Laplace transform. Crucially, we proved both the uniqueness and conditional stability of the inverse source problem given interior measurements on a subdomain. The efficacy of the proposed approach was corroborated by numerical benchmarks, which confirmed that L-PINNs provide a robust and accurate computational strategy for this class of fractional inverse problems.

It should be noted that the theoretical analysis and the proposed L-PINNs framework rely on Assumption 1, which assumes analyticity of the source term. While this covers a broad class of problems, future work will explore extensions to more general source terms, such as finite-time or pulsed sources, and investigate the corresponding numerical stability of the Laplace inversion process.

Use of AI tools declaration

The authors declare they have not used Artificial Intelligence (AI) tools in the creation of this article.

Acknowledgments

Research work of Changxin Qiu was partially supported by the Zhejiang Provincial Natural Science Foundation of China under Grant No. LMS26A010009, NSFC Grant No. 12201327, and the Natural Science Foundation of Ningbo Municipality No. 2022J087. Research work of Zhiyuan Li was partially supported by NSFC Grant No. 12271277 and the Natural Science Foundation of Ningbo Municipality No. 2024QL045 and was partly supported by the Open Research Fund of Key Laboratory of Nonlinear Analysis & Applications (Central China Normal University), Ministry of Education, China.

Conflict of interest

The authors declare there are no conflicts of interest.

References

1. V. Kulish, J. Lage, Application of fractional calculus to fluid mechanics, *J. Fluids Eng.*, **124** (2002), 803–806. https://doi.org/10.1115/1.1478062
2. R. Magin, Fractional calculus models of complex dynamics in biological tissues, *Comput. Math. Appl.*, **59** (2010), 1586–1593. https://doi.org/10.1016/j.camwa.2009.08.039
3. D. del Castillo-Negrete, B. A. Carreras, V. E. Lynch, Fractional diffusion in plasma turbulence, *Phys. Plasmas*, **11** (2004), 3854–3864. https://doi.org/10.1063/1.1767097
4. J. Singh, D. Kumar, D. Baleanu, On the analysis of chemical kinetics system pertaining to a fractional derivative with mittag-leffler type kernel, *Chaos*, **27** (2017), 103113. https://doi.org/10.1063/1.4995032
5. J. Ren, Z. Sun, W. Dai, New approximations for solving the caputo-type fractional partial differential equations, *Appl. Math. Modell.*, **40** (2016), 2625–2636. https://doi.org/10.1016/j.apm.2015.10.011
6. J. Huang, Y. Tang, L. Vázquez, J. Yang, Two finite difference schemes for time fractional diffusion-wave equation, *Numerical Algorithms*, **64** (2013), 707–720. https://doi.org/10.1007/s11075-012-9689-0
7. S. Kheybari, Numerical algorithm to Caputo type time–space fractional partial differential equations with variable coefficients, *Math. Comput. Simul.*, **182** (2021), 66–85. https://doi.org/10.1016/j.matcom.2020.10.018
8. C. Li, Z. Wang, The local discontinuous galerkin finite element methods for caputo-type partial differential equations: mathematical analysis, *Appl. Numer. Math.*, **150** (2020), 587–606. https://doi.org/10.1016/j.apnum.2019.11.007
9. H. Fahad, A. Fernandez, Operational calculus for caputo fractional calculus with respect to functions and the associated fractional differential equations, *Appl. Math. Comput.*, **409** (2021), 126400. https://doi.org/10.1016/j.amc.2021.126400
10. S. Sivalingam, P. Kumar, H. Trinh, V. Govindaraj, A novel l1-predictor-corrector method for the numerical solution of the generalized-caputo type fractional differential equations, *Math. Comput. Simul.*, **220** (2024), 462–480. https://doi.org/10.1016/j.matcom.2024.01.017
11. X. Huang, Y. Kian, É. Soccorsi, M. Yamamoto, Determination of source or initial values for acoustic equations with a time-fractional attenuation, *Anal. Appl.*, **21** (2023), 1105–1130. https://doi.org/10.1142/S0219530523500100
12. D. Jiang, Y. Liu, M. Yamamoto, Inverse source problem for the hyperbolic equation with a time-dependent principal part, *J. Differ. Equations*, **262** (2017), 653–681. https://doi.org/10.1016/j.jde.2016.09.036

13. Y. Liu, D. Jiang, M. Yamamoto, Inverse source problem for a double hyperbolic equation describing the three-dimensional time cone model, *SIAM J. Appl. Math.*, **75** (2015), 2610–2635. https://doi.org/10.1137/15M1018836

14. Y. Zhang, X. Xu, Inverse source problem for a fractional diffusion equation, *Inverse Probl.*, **27** (2011), 035010. https://doi.org/10.1088/0266-5611/27/3/035010

15. P. Niu, T. Helin, Z. Zhang, An inverse random source problem in a stochastic fractional diffusion equation, *Inverse Probl.*, **36** (2020), 045002. https://doi.org/10.1088/1361-6420/ab532c

16. D. Jiang, Z. Li, Y. Liu, M. Yamamoto, Weak unique continuation property and a related inverse source problem for time-fractional diffusion-advection equations, *Inverse Probl.*, **33** (2017), 055013. https://doi.org/10.1088/1361-6420/aa58d1

17. J. Janno, Y. Kian, Inverse source problem with a posteriori boundary measurement for fractional diffusion equations, *Math. Methods Appl. Sci.*, **46** (2023), 15868–15882. https://doi.org/10.1002/mma.9432

18. W. Wang, M. Yamamoto, B. Han, Numerical method in reproducing kernel space for an inverse source problem for the fractional diffusion equation, *Inverse Probl.*, **29** (2013), 095009. https://doi.org/10.1088/0266-5611/29/9/095009

19. J. Wang, Y. Zhou, T. Wei, Two regularization methods to identify a space-dependent source for the time-fractional diffusion equation, *Appl. Numer. Math.*, **68** (2013), 39–57. https://doi.org/10.1016/j.apnum.2013.01.001

20. X. Cheng, Z. Li, Uniqueness and stability for inverse source problem for fractional diffusion-wave equations, *J. Inverse Ill-Posed Probl.*, **31** (2021), 885–904. https://doi.org/10.1515/jiip-2021-0078

21. Y. Liu, G. Hu, M. Yamamoto, Inverse moving source problem for time-fractional evolution equations: determination of profiles, *Inverse Probl.*, **37** (2021), 084001. https://doi.org/10.1088/1361-6420/ac0c20

22. K. Liao, T. Wei, Identifying a fractional order and a space source term in a time-fractional diffusion-wave equation simultaneously, *Inverse Probl.*, **35** (2019), 115002. https://doi.org/10.1088/1361-6420/ab383f

23. X. Yan, T. Wei, Determine a space-dependent source term in a time fractional diffusion-wave equation, *Acta Appl. Math.*, **165** (2020), 163–181. https://doi.org/10.1007/s10440-019-00248-2

24. M. Yamamoto, Uniqueness for inverse source problems for fractional diffusion-wave equations by data during not acting time, *Inverse Probl.*, **39** (2023), 024004. https://doi.org/10.1088/1361-6420/aca55c

25. M. Lassas, Z. Li, Z. Zhang, Well-posedness of the stochastic time-fractional diffusion and wave equations and inverse random source problems, *Inverse Probl.*, **39** (2023), 084001. https://doi.org/10.1088/1361-6420/acdab9

26. B. Jin, W. Rundell, A tutorial on inverse problems for anomalous diffusion processes, *Inverse Probl.*, **31** (2015), 035003. https://doi.org/10.1088/0266-5611/31/3/035003

27. L. Guo, H. Wu, X. Yu, T. Zhou, Monte carlo fpinns: Deep learning method for forward and inverse problems involving high dimensional fractional partial differential equations, *Comput. Methods Appl. Mech. Eng.*, **400** (2022), 115523. https://doi.org/10.1016/j.cma.2022.115523

28. G. Pang, L. Lu, G. Karniadakis, fpinns: Fractional physics-informed neural networks, *SIAM J. Sci. Comput.*, **41** (2019), A2603–A2626. https://doi.org/10.1137/18M1229845
29. J. Hou, Z. Ma, S. Ying, Y. Li, HNS: An efficient hermite neural solver for solving time-fractional partial differential equations, *Chaos, Solitons Fractals*, **181** (2024), 114637. https://doi.org/10.1016/j.chaos.2024.114637
30. Z. Ma, J. Hou, W. Zhu, Y. Peng, Y. Li, Pmnn: Physical model-driven neural network for solving time-fractional differential equations, *Chaos, Solitons Fractals*, **177** (2023), 114238. https://doi.org/10.1016/j.chaos.2023.114238
31. Z. Chen, C. Qiu, Z. Li, S. Xu, Laplace-based physics-informed neural networks for solving nonlinear coefficient inverse problem for acoustic equation with fractional derivative, *Phys. Fluids*, **37**, (2025), 077198. https://doi.org/10.1063/5.0278224
32. H. Qu, X. Liu, Z. She, Neural network method for fractional-order partial differential equations, *Neurocomputing*, **414** (2020), 225–237. https://doi.org/10.1016/j.neucom.2020.07.063
33. H. Qu, Z. She, X. Liu, Neural network method for solving fractional diffusion equations, *Appl. Math. Comput.*, **391** (2021), 125635. https://doi.org/10.1016/j.amc.2020.125635
34. S. Wang, H. Zhang, X. Jiang, Fractional physics-informed neural networks for time-fractional phase field models, *Nonlinear Dyn.*, **110** (2022), 2715–2739. https://doi.org/10.1007/s11071-022-07746-3
35. S. Wang, H. Zhang, X. Jiang, Physics-informed neural network algorithm for solving forward and inverse problems of variable-order space-fractional advection–diffusion equations, *Neurocomputing*, **535** (2023), 64–82. https://doi.org/10.1016/j.neucom.2023.03.032
36. Z. Hajimohammadi, F. Baharifard, A. Ghodsi, K. Parand, Fractional chebyshev deep neural network (fcdnn) for solving differential models, *Chaos, Solitons Fractals*, **153** (2021), 111530. https://doi.org/10.1016/j.chaos.2021.111530
37. K. Sakamoto, M. Yamamoto, Initial value/boundary value problems for fractional diffusion-wave equations and applications to some inverse problems, *J. Math. Anal. Appl.*, **382** (2011), 426–447. https://doi.org/10.1016/j.jmaa.2011.04.058
38. I. Podlubny, *Fractional Differential Equations, An Introduction to Fractional Derivatives*, Academic Press, 1998.
39. J. Gaver, P. Donald, Observing stochastic processes, and approximate transform inversion, *Oper. Res.*, **14** (1966), 444–459. https://doi.org/10.1287/opre.14.3.444
40. X. Yan, Z. Xu, Z. Ma, Laplace-fpinns: Laplace-based fractional physics-informed neural networks for solving forward and inverse problems of subdiffusion, preprint, arXiv:2304.00909.
41. C. Li, F. Zeng, *Numerical methods for fractional calculus*, CRC Press, New York, 2015.

AIMS Press